J. Fluid Mech. (1985), *vol.* 153, *pp.* 229–242
Printed in Great Britain

Comparison of direct numerical simulation of two-dimensional turbulence with two-point closure: the effects of intermittency

By J. R. HERRING AND J. C. McWILLIAMS
Geophysical Turbulence Program, National Center for Atmospheric Research, Boulder, Colorado 80307

(Received 6 March 1984 and in revised form 13 October 1984)

We compare results of high-resolution direct numerical simulation with equivalent two-point moment closure (the test-field model) for both randomly forced and spin-down problems. Our results indicate that moment closure is an adequate representation of observed spectra only if the random forcing is sufficiently strong to disrupt the dynamical tendency to form intermittent isolated vortices. For strong white-noise forcing near a lower-wavenumber cut-off, theory and simulation are in good agreement except in the dissipation range, with an enstrophy range less steep than the wavenumber to the minus fourth power. If the forcing is weak in amplitude, red noise, and at large wavenumbers, significant errors are made by the closure, particularly in the inverse-cascade range. For spin-down problems at large Reynolds numbers, the closure considerably overestimates enstrophy transfer to small scales, as well as energy transfer to large scales. We finally discuss the possibility that the closure errors are related to intermittency of various types. Intermittency can occur in either the inverse-cascade range (forced equilibrium) or the intermediate scales (spin-down), with isolated concentrations of vorticity forming the associated coherent structures, or it can occur in the dissipation range owing to the nonlinear amplification of variations in the cascade rate (Kraichnan 1967).

1. Introduction and summary

Several independent studies (Fornberg 1977; Basedevant *et al.* 1981; McWilliams 1984*a*, 1984*b*) suggest that high-Reynolds-number two-dimensional turbulence may – in certain circumstances – evolve in such a manner that there is little (or asymptotically no) enstrophy flux to small scales. This can occur due to the presence of dynamically stable, isolated vorticity concentrations (vortices; see figure 10), either in spin-down flows, where they arise from random, Gaussian initial conditions, or in equilibrium flows with random forcing. In these cases the flow departs substantially from Gaussianity. This condition is inhospitable to moment closures – such as the Test Field Model (TFM) of Kraichnan (1971). In order to gain insight into the magnitude of this problem, we compare direct numerical simulations (DNS) (spectral, mostly 256×256) with equivalent closure (TFM) for a variety of forcing functions, including spin-down (i.e. no forcing). The DNS solutions compared here have been described in McWilliams (1984).

Our results for forced cases are that the closure may be quantitatively accurate only if the disruptive effects of random stirring are sufficiently strong to prevent the formation of coherent structures natural to two-dimensional turbulence. The disruptive effects are maximal for strong forcing near the low-wavenumber cut-off.

Our numerical study of such a forced system shows the DNS and TFM to be in close agreement over the entire enstrophy inertial range, but a significant discrepancy still exists in the dissipation range for high resolution and high Reynolds numbers. If, on the other hand, the forcing is at sufficiently high wavenumbers and is correspondingly weak so as to permit the possibility for an appreciable inverse cascade, the closure appears to considerably overestimate the flux in the inverse-cascade range. The actual cascade is considerably reduced by the emergence of isolated vortices, which cascade little energy to large scales. Such isolated vortices may be an expression of large-scale intermittency, as anticipated by Kraichnan (1975). Our results in this case may be compared to those of Basedevant *et al.* (1981), who also find evidence for isolated vortices in their 128×128 simulations. These authors also report kinetic-energy spectra considerably steeper than wavenumber to the minus third power, and suggest a connection between the intermittency and spectral slope. Our TFM results suggest caution in this identification in that the TFM also has a similarly steep slope but, of course, no isolated structures. Hence this wavenumber span (1, 64) is too small to make accurate statements about asymptotic (i.e. infinite resolution and Reynolds number) spectral shapes.

For freely decaying turbulence at large Reynolds numbers, the closures and numerical simulations remain in quantitative agreement only for a few large-eddy turnover times. This is the same as the time to build up high-order correlations (cumulants) in the flow. After this time, the actual flow evolves to a state which consists of isolated vortices which continue to coalesce intermittently. This state is characterized statistically as having quite high values of the vorticity kurtosis (~ 40), and steep spectra (significantly steeper than k^{-4} at high wavenumbers k).

Our DNS results may be compared with recent calculations of Brachet & Sulem (1984), who have reported extremely high-resolution (1024×1024) calculations which show a consistency with a log-modified k^{-3} spectrum for decaying two-dimensional turbulence. Such high resolution was reached by the use of a sparse spectral method which assumed a certain symmetry that is preserved in the nonlinear evolution (i.e. vorticity is odd-symmetric about both midlines of the domain, $x = \pi$ and $y = \pi$). The initial state in this study consisted of only a few large-scale wavenumbers. The time interval studied reached only just past the point at which the enstrophy flux became maximum, which is a time before the coherent vortex component of the flow would become dominant. They further showed that lower resolutions were unable to resolve a 'viscous instability', which is vital for the development of a k^{-3} enstrophy range. Our DNS results are clearly below this limit. Without delving into the subtleties of large-wavenumber instabilities, we simply note that we here compare TFM and DNS for equivalent conditions (same resolution); thus any discrepancy between the two should be real, unless it were argued that the closure relies tacitly for its validity on the viscous instability. Their assumption of a particular spectrum symmetry is not germane to our differences, because we have verified that our DNS results are qualitatively unchanged with this symmetry.

2. Description of calculations performed: DNS and TFM

We consider a flow confined in a periodic square box (with sides L) whose vorticity $\xi(\boldsymbol{x}, t)$ satisfies

$$\frac{\partial\{\xi\}(\boldsymbol{k})}{\partial t} = \{\mathrm{J}(\psi, \xi)\}(\boldsymbol{k}) - \nu(k)\{\xi\}(\boldsymbol{k}, t) + F(\boldsymbol{k}, t). \tag{1}$$

Here J is the Jacobian, ψ the stream function, $k = |\boldsymbol{k}|$, and $\{a\}(\boldsymbol{k})$ denotes the Fourier transform of a. The dissipation function $\nu(k)$ is here taken as

$$\nu(k) = \nu_0 + \nu_4 k^4. \tag{2}$$

$F(\boldsymbol{k}, t)$ is a random force whose form is a narrow pulse in wavenumber k. The specific form used here is

$$F(\boldsymbol{k}, t) = f_k(\boldsymbol{k}) f_t(t), \tag{3}$$

where $$\langle f_k(\boldsymbol{k}) f_k(-\boldsymbol{k})\rangle = A(k-k_1)_+^4 (k_2-k)_+^4/k^2 = A\sigma(k_1, k_2, k)$$

and $$\langle f_t(t) f_t(t')\rangle = \eta \exp(-\eta|t-t'|).$$

Here $\langle\ \rangle$ means ensemble average. In (3) our notation is that

$$(x)_+ = \begin{cases} x & (x > 0), \\ 0 & (x \leqslant 0). \end{cases}$$

The method used to solve (1)–(3) is described briefly in McWilliams (1984*a*, 1984*b*) and will be described in more detail in Haidvogel (1985). These equations are solved collocatively, using complex exponentials as a basis. The box periodicity length $L = 2\pi$. This implies a lower wavenumber cut-off of $k_{\min} = 1$ and a unit wavenumber discretization interval. For most of the cases considered below, the spatial grid resolution is 256, which implies that the largest wavenumber admitted is $k_{\max} = 128$. Time-stepping is by leapfrog, with a periodic Crank–Nicholson time-step to suppress instability.

The TFM closure equation with which the DNS is to be compared has been described by Kraichnan (1972) and by Herring *et al.* (1974). We refer the reader to those papers for a detailed account of the energy-spectrum equations of motion. Here we simply recall that the TFM is of the eddy-sampled quasi-normal Markovian form (Orszag 1974), with the eddy-damping rate – which determines the relaxation of triple moments – prescribed as the rate at which a compressible test field exchanges excitation between its compressive and solenoidal components if convected by the actual velocity field. The theory contains a single arbitrary constant, whose value was previously determined by comparisons with DNS (Herring *et al.* 1974). This constant ($g^2 = 0.60$) represents the efficiency of pressure scrambling in de-correlating triple moments.

We remark that the DNS and TFM also differ in that the TFM is solved by approximating lattice sums by approximating integrals on the interval $(k_{\min}, k_{\max})$. This difference may be significant if there is an appreciable amount of energy near $k_{\min}$, a condition which we avoid in making comparisons between theory and simulations.

Table 1 lists the runs investigated in this paper. The last of these is a spin-down problem in which the initial energy spectrum $E(k, 0)$ is

$$E(k, 0) = \frac{72}{\pi} \frac{k}{6^4 + k^4}, \tag{4}$$

where the amplitude is such that

$$\int_0^\infty \mathrm{d}k\, E(k, 0) = \tfrac{1}{2}.$$

Case	ν_0	ν_4	$k_{\min}$	$k_{\max}$	η	A	k_1	k_2
1 (*a*)	0.10	5.000×10^{-7}	1	64.0	$1/\Delta t\sim\infty$†	0.20000	1.19	4.877
1 (*b*)	0.10	5.000×10^{-8}	1	128.0	$1/\Delta t\sim\infty$‡	0.100	1.19	4.877
2	0.05	5.000×10^{-8}	1	128.0	0.231	0.00705	18.5	21.5
3	0.00	3.125×10^{-8}	1	128.0	—	0.00000	—	—

† $\Delta t = 4\times10^{-3}$ for the DNS.
‡ $\Delta t = 2\times10^{-3}$ for the DNS.

TABLE 1

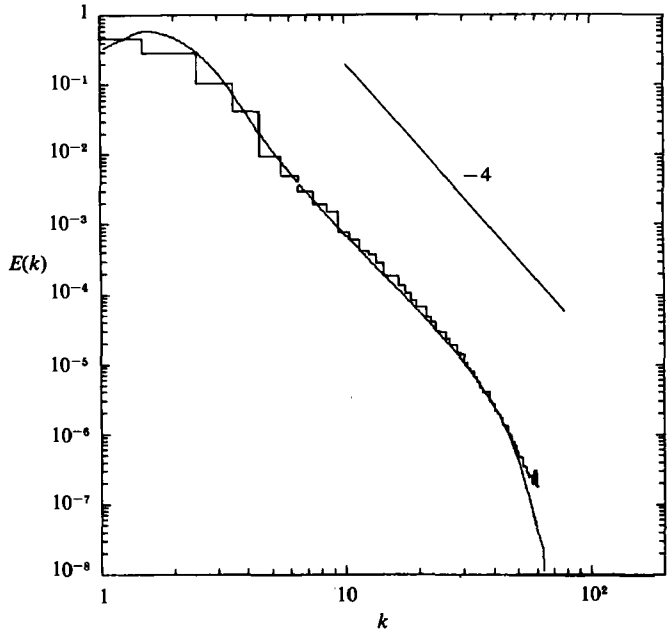

FIGURE 1. Energy spectrum $E(k)$ for case 1 (*a*) ($1 \leqslant k \leqslant 164$) in the stationary state.

3. Results

We discuss first the equilibrium cases 1 and 2, considering first the low-wavenumber forcing cases 1 (*a*, *b*). Comparison of the stationary-state value of energy spectra $E(k) = 2\pi k\langle\{\xi\}(\boldsymbol{k}, t)\{\xi\}(-\boldsymbol{k}, t)/k^2\rangle/2$ is presented in figures 1 and 2 for cases 1 (*a*, *b*). For the low-resolution case 1 (*a*) the agreement between TFM (smooth) and time-averaged DNS (histogram) is quite satisfactory. This case has only an enstrophy-cascade range; the forcing is close to the lower-wavenumber cut-off, allowing no space for inverse cascade. The temporal fluctuations in total energy $E(t)$ and total enstrophy $V(t) = \frac{1}{2}\langle|\xi(\boldsymbol{x}, t)|^2\rangle$ (shown in figures 3 and 4) are quite violent; this is due to the white-noise driving $F(k, t)$ for this case. $E(k)$ is not quite as steep as k^{-4}, although $\nu_0 \neq 0$. The DNS considered here is quite similar – in its forcing and wavenumber range – to the calculation of Basedevant *et al.* (1981). The slope d ln $E(k)$)/d ln k is rather close to -4 for both DNS and TFM. We attribute the excessive steepness relative to the closure theory's asymptotic form of $k^{-3}/(\ln(k))^{\frac{2}{3}}$ to the limited wavenumber range (1, 64); we were unable with this range to demonstrate the (log-modified) k^{-3} asymptotic TFM range for any forcing and dissipation law. Our

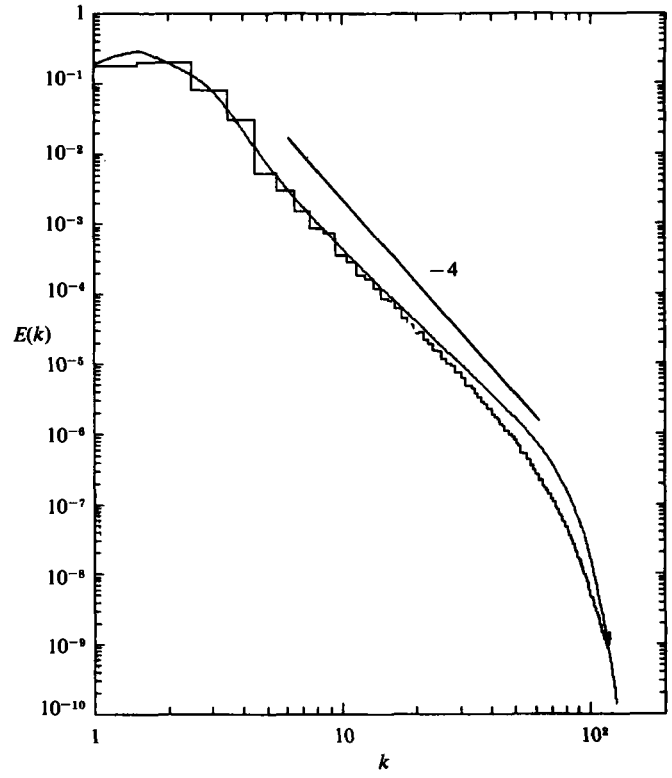

FIGURE 2. Energy spectrum $E(k)$ for case 1(*b*) ($1 \leqslant k \leqslant 128$) in the stationary state.

point here is that it appears difficult to discern between intermittency and limited resolution as to the cause of the steepening of the spectral slope.

Spectral results for the high-resolution ($1 \leqslant k \leqslant 128$), low-wavenumber forcing (case 1*b*) are presented in figure 2. Here, good agreement is obtained in the enstrophy inertial range, but the TFM overpredicts the dissipation-range excitation by about a factor of 2. The trend of this overprediction is the same as in Herring *et al.* (1974), but the magnitude is much larger. We note that the DNS small-scale Reynolds number (Re_2, see (10*b*) and table 2) is twice that of TFM for case 1*b*, suggesting a progressive TFM overprediction of energy in the inertial range with increasing Re_2. The TFM difference – in proceeding from case 1(*a*) ($1 \leqslant k \leqslant 64$) to case 1(*b*) ($1 \leqslant k \leqslant 128$) is consistent with a tendency for the theory to asymptote (as $Re_2 \to \infty$) toward a k^{-3} range just prior to entering – with increasing k – the dissipation range. This may or may not be so for the DNS. Also for the latter, the presence of appreciable intermittency undoubtedly lowers the dissipation range, as in the earlier numerical studies of McWilliams & Chow (1979), and as predicted by Kraichnan (1967) and by Frisch & Morf (1981).

Case 2 allows for an appreciable inverse-cascade range $(k_{\min}, k_f) = (1, 20)$, where $k_f = \frac{1}{2}(k_1 + k_2)$. In addition, the forcing is non-white, which – strictly speaking – takes us outside the domain of the TFM. We must therefore give a prescription for an effective forcing of $V(k) = \frac{1}{2}\langle|\{\xi\}(\boldsymbol{k}, t)|^2\rangle$. It is

$$F_V(k) = \frac{A\sigma(k_1, k_2, k)\tau}{1+\tau\eta}, \tag{5}$$

$$\tau(k) = \frac{\pi^{\frac{1}{2}}}{2kE^{\frac{1}{2}}}.$$

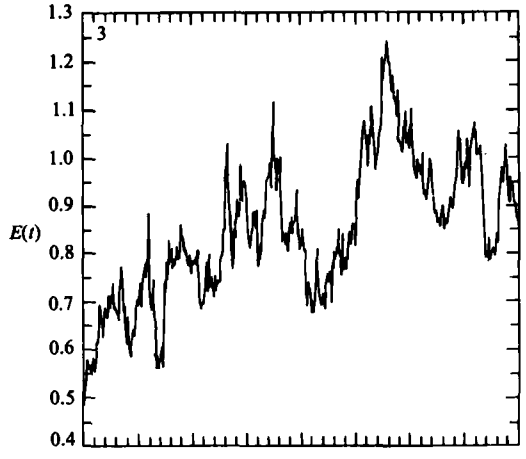

FIGURE 3. Total energy $E(t)$ for case 1 (a). $E(k)$ (figure 1) is obtained only from the stationary phase ($20 \leqslant t \leqslant 40$).

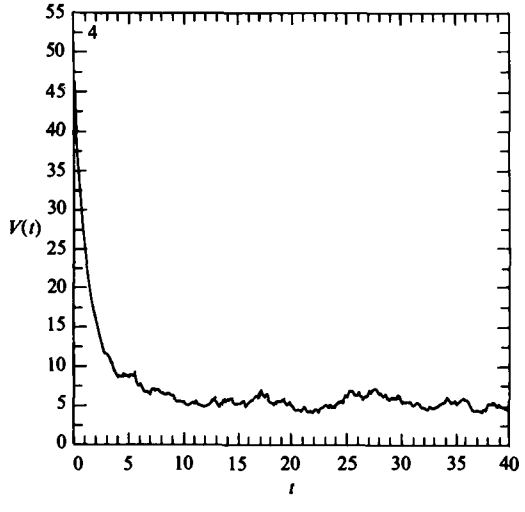

FIGURE 4. Total enstrophy $V(t)$ for case 1 (a).

Here η is the timescale of the random forcing, as in table 1. For the parameter range of case 2, $\tau\eta \ll 1$ and may be neglected. Equation (5) is obtained by solving, on a short timescale,

$$\frac{\partial\{\xi\}(\boldsymbol{k})}{\partial t} = F(\boldsymbol{k},t) + \boldsymbol{u}_0 \cdot \boldsymbol{k}\{\xi\}(\boldsymbol{k},t) - \nu(k)\{\xi\}(\boldsymbol{k},t). \tag{6}$$

Equation (5) is correct if it is valid to assume that all but a negligible part of the energy is at scales much larger than k and that the effect of $\{\boldsymbol{u}\}(\boldsymbol{k},t)$ on V may be replaced by a Gaussian large-scale field $\boldsymbol{u}_0(t)$, whose timescale is fast compared with that of the forcing.

DNS and TFM comparisons for stationary $E(k)$ in case 2 are given in figure 5. We notice an appreciable discrepancy in the inverse-cascade range, where the emergence of vortex structures in the simulation appears to arrest the inverse cascade. Despite this fact, the DNS and TFM have a strong intimation of a $k^{-\frac{5}{3}}$ range. Our results in this regard are in qualitative agreement with the recent calculations of Frisch & Sulem (1984). It is possible to estimate from figure 5 a Kolmogorov constant. Thus

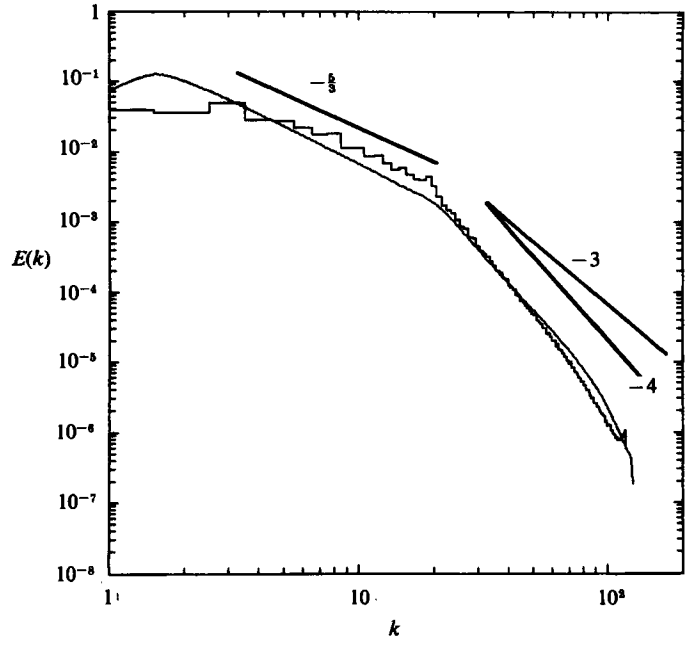

FIGURE 5. Energy spectrum for stationary phase of case 2.

Case	E	V	S	K_ψ	K_ξ	Re_1	Re_2
1 (*a*) TFM	1.000	5.91	0.613	—	—	12.1	6116
1 (*a*) DNS	0.936	4.90	0.767	~ 3	~ 3	11.0	4620
1 (*b*) TFM	0.500	3.31	1.06	—	—	9.09	11855
1 (*b*) DNS	0.512	3.11	0.776	~ 3	~ 3	8.81	23300
2 TFM	0.378	25.9	0.776	—	—	76.4	595.4
2 DNS	0.352	37.7	0.504	~ 3	~ 9	52.7	680

TABLE 2

the maximum of $k^{\frac{5}{3}}E(k)/\epsilon$ ($\epsilon \equiv$ the energy flux to large scales) is 4.8 for DNS and 2.9 for TFM. However, we should stress that these estimates are far from asymptotic; recall Kraichnan's value of 6.5 from the TFM at $Re = \infty$ for $g = 1$ (note that the $k^{-\frac{5}{3}}$ coefficient $\sim g^{\frac{4}{3}}$ in the TFM). They are consistent with those of Lilly (1969), ~ 4.3–6.2, but much smaller than those of Siggia & Aref (1981), ~ 14. In the enstrophy cascade and dissipation ranges the comparison is slightly more satisfactory, although the TFM is too shallow (as in case 1 *b*).

Figures 6 and 7 show $E(t)$ and $V(t)$ for case 2, during a significant portion of the stationary phase of the flow. Note the much attenuated noise level as compared to figures 3 and 4, for case 1. In part, this reduction is due to the non-Gaussian method of forcing (Markovian, with memory time η^{-1}).

Table 2 compares integral parameters E, V and S for cases 1 and 2. Here S is

$$S(t) = \frac{2\left\langle\left(\frac{\partial\xi}{\partial x}\right)^2\frac{\partial u}{\partial x}\right\rangle}{\left\langle\left(\frac{\partial\xi}{\partial x}\right)^2\right\rangle\left\langle\left(\frac{\partial u}{\partial x}\right)^2\right\rangle^{\frac{1}{2}}}. \tag{7a}$$

In the statistically steady state, we note that, according to (1), $S(t)$ is equal to $S'(t)$, where

$$S'(t) = \frac{2\int_0^\infty \mathrm{d}k\, \nu(k)\, k^4 E(k)}{\left\langle \left(\frac{\partial \xi}{\partial x}\right)^2 \right\rangle \left\langle \left(\frac{\partial u}{\partial x}\right)^2 \right\rangle^{-\frac{1}{2}}}, \tag{7b}$$

where we assume that the contribution from the random forcing may be neglected, as may occur in practical cases for which there is forcing at small k and dissipation at large k. Even for decaying flows, we may expect a rough equality $S(t) \approx S'(t)$, since their main contribution comes from large k, where relaxational effects are strong.

We note that S is a lowest-order measure (in the sense of cumulants) of non-Gaussian statistics of the flow field. Perhaps more significant and descriptive measures are the kurtosis of stream function and vorticity defined by

$$K_\psi = \frac{\langle [\psi(\boldsymbol{x}, t)]^4 \rangle}{(\langle [\psi(\boldsymbol{x}, t)]^2 \rangle)^2}, \tag{8}$$

$$K_\xi = \frac{\langle [\xi(\boldsymbol{x}, t)]^4 \rangle}{(\langle [\xi(\boldsymbol{x}, t)]^2 \rangle)^2}. \tag{9}$$

These quantities measure directly the spatial intermittency of the fields ψ and ξ, but their dynamical significance is not immediate. The Gaussian value is 3. K_ψ and K_ξ are also listed in table 2 for cases 1 and 2 in the DNS; they are not listed for the TFM since they are not computed by this theory.

Finally, we define Reynolds numbers suitable for the total viscosity and the hyperviscosity component in (2) by

$$Re_1 = \frac{E(t)\, V^{\frac{1}{2}}}{\int_0^\infty \mathrm{d}k\, \nu(k)\, E(k)}, \tag{10a}$$

$$Re_2 = \frac{E(t)\, V^{\frac{1}{2}}}{\int_0^\infty \mathrm{d}k\, \nu_4 k^4\, E(k)}. \tag{10b}$$

Here V is the enstrophy, Re_1 is a large-scale Reynolds number, while Re_2 is sensitive to the small scales. Values for Re_1 and Re_2 are also listed in table 2. We noted above that the TFM closure does not make predictions for the K's. However, a derivation of TFM via perturbation theory (Kraichnan 1971) is clearly better justified for flows whose statistics are near-Gaussian. The agreement between DNS and TFM for the second-order moments listed in table 2 is typical of the agreement for earlier lower-resolution calculations (Herring *et al.* 1974). The agreement between S(DNS) and S(TFM) for case 2 is somewhat surprising. Also, note that our microscale Reynolds number Re_2 is much larger – for both DNS and TFM – than the large-scale Re_1.

Let us now examine the spin-down run, case 3, where $F = \nu_0 = 0$. A complete descriptive account of this flow – including the emergence of isolated vortices and their agglutination – is to be found in McWilliams (1984). We here focus only on those aspects of the flow predicted by the closure. Figure 8 presents a comparison of DNS and TFM predictions for the energy, enstrophy, skewness (see (7)) and effective Reynolds number Re (see (10a)) (note that $Re_1 = Re_2$ for this case). In estimating the

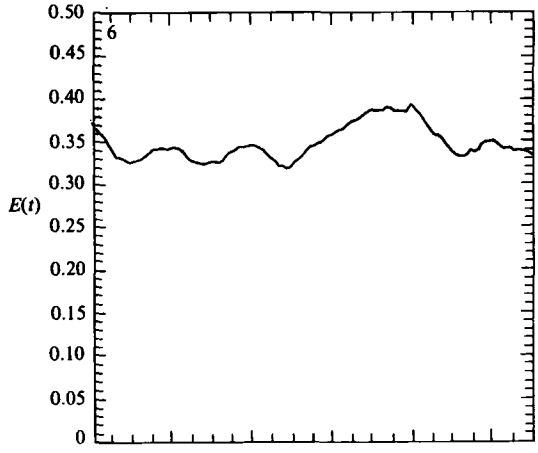

FIGURE 6. Total energy $E(t)$ for case 2. Spectrum for case 2 is obtained as time average over $(80 \leqslant t \leqslant 160)$.

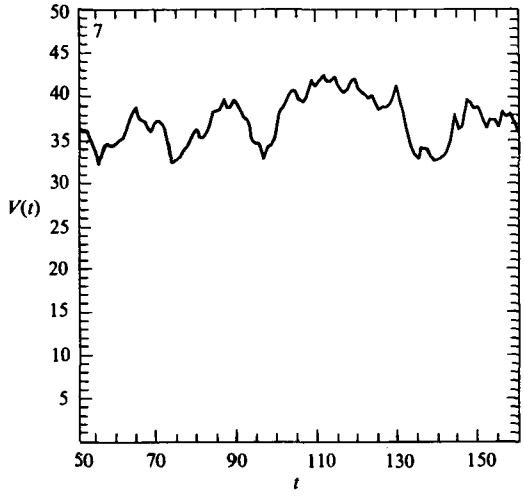

FIGURE 7. Total enstrophy $V(t)$ for case 2.

skewness we use (7*b*) instead of (7*a*), since the latter is not conveniently available from the DNS run. As noted earlier, in equilibrium, these are equal. In the present TFM decay solution the former exceeds the latter by about 20 %.

Generally, for case 3 the TFM gives a poor forecast of these quantities. A close examination shows that with the exception of $S'(t)$ – whose trend is poor even at small t – the TFM values are accurate for $t < 2$–3, and rapidly deteriorate as t increases beyond $t = 5$. This is borne out in more detail on the spectral plots for $E(k, t)$, presented in figures 9(*a–d*). Beyond $t = 10$ the TFM $E(k, t)$ tends rapidly toward a singular distribution, with virtually all energy in the largest-available scale (i.e. $k = 1$). For the TFM the $(1 \leqslant k \leqslant 2)$ range of wavenumbers develops a negative eddy viscosity for $t > 5$, feeding energy into the lowest-available mode ($k = 1$), causing it to grow exponentially at the expense of all other modes at least on the timescale relevant to the present discussion. (By eddy viscosity we mean here the term proportional to $E(k, t)$ in the TFM's evaluation of the energy-transfer function; there is no empirical constant needed for its evaluation.) For $t < 5$ the TFM eddy viscosity

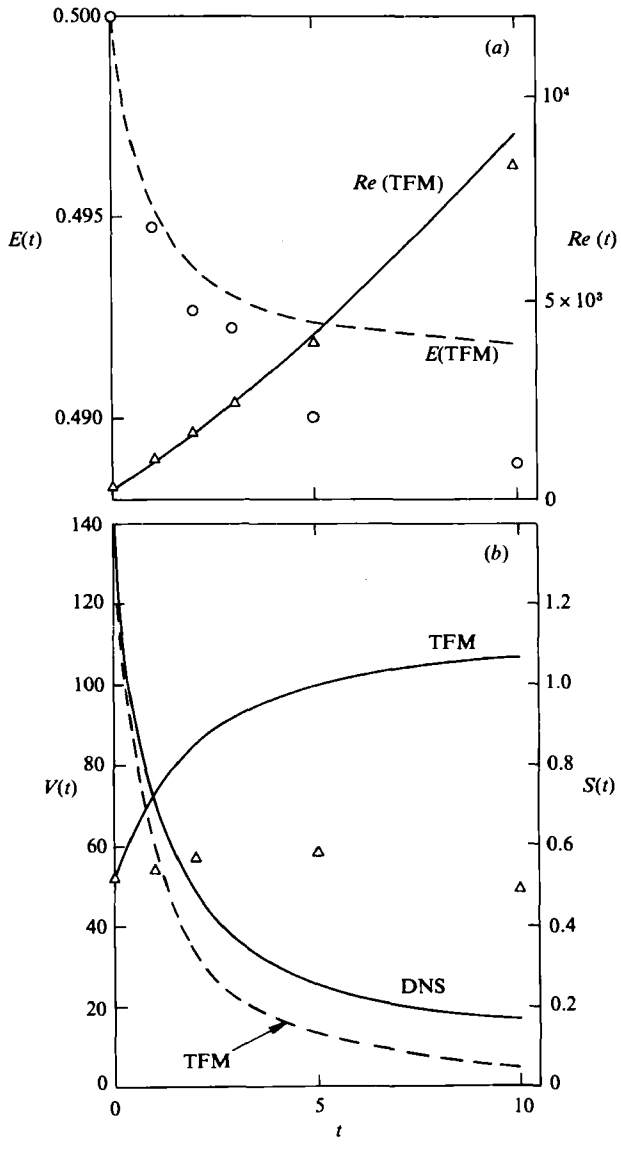

FIGURE 8. (*a*) Total energy $E(t)$ and effective Reynolds number $Re(t)$ for decaying turbulence, case 3. Ordinate for $Re(t)$ is at the right. For TFM, $E(t)$ is a dashed line and $R(t)$ is a solid line. For DNS, $E(t)$ is represented by open circles and $Re(t)$ open triangles. (*b*) Total enstrophy $V(t)$ and skewness $S'(t)$ (see (7*b*)) for case 3 as function of time. Ordinate for $S'(t)$ is at right. For TFM, $V(t)$ is a dashed line, and $S'(t)$ solid. For DNS, $V(t)$ is a solid line, and $S'(t)$ open triangles. The unit of time corresponds to $0.728L/u$, where L is the integral scale and u the r.m.s. velocity at $t = 0$.

is positive for all k. Furthermore, the $E(k, t)$ computed on a continuous wavenumber span ($0 < k < 128$) is virtually identical with that of the present run for $t < 10$; significant differences do occur for $t > 10$. The above system has no negative eddy viscosity. We have no means of assessing the value of the eddy viscosity concept for the DNS. We should note, however, that in the present context Kraichnan's (1975) demonstration that the TFM's eddy viscosity is negative is valid only if there exists a low-wavenumber cutoff, and if in addition wavenumber lattice-sums are replaced

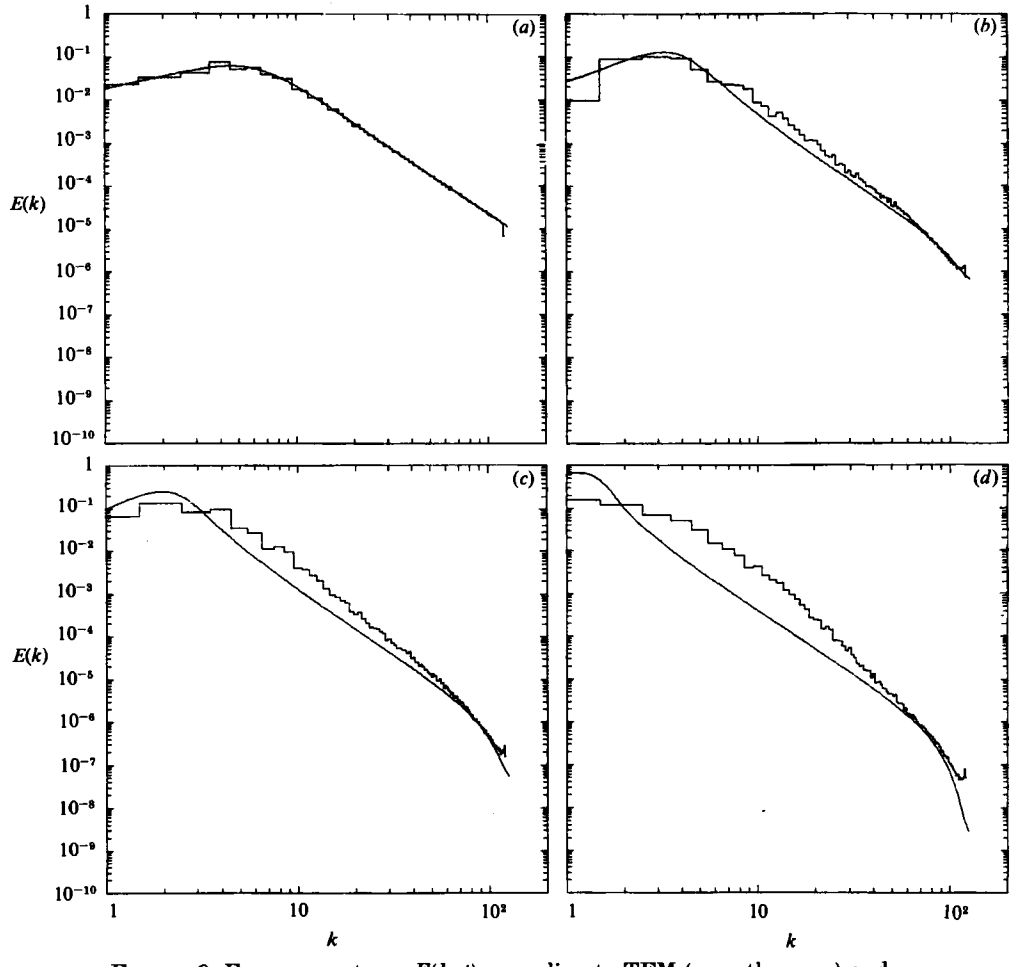

FIGURE 9. Energy spectrum $E(k, t)$ according to TFM (smooth curve) and DNS (histogram) selected values of t: (*a*) 0; (*b*) 2; (*c*) 5; (*d*) 10.

by approximating integrals. These considerations suggest that for $t < 10$ wavenumber discretization errors are small; discrepancies between TFM and DNS are thus a result of the TFM's erroneous dynamics. Beyond $t = 10$ we are not certain how to apportion the TFM–DNS difference between dynamical error and low-k discretization error.

Excepting the range $1 < k < 2$ – where the lack of many available wavenumbers, and hence the large statistical scatter, in the DNS precludes any certain conclusion – the case 3 discrepancy may be summarized as follows: the TFM overpredicts the amount of energy transferred to smaller k, yielding an excess of $E(k)$ in the DNS at the k-values approximately corresponding to the coherent structures. (One must be cautious in assigning the vortices to a particular k-range; their partitioning in $E(k)$ is based not only on their range of sizes but also on their range of separations.) The extent of discrepancy in $E(k)$ increases in time. The time for the development of strong DNS–TFM difference seems to be the same for the development of strong departure of K_ξ from Gaussianity.

Figure 10 shows the DNS vorticity field for case 3 at $t = 10$. Note the intense isolated vortices, separated by regions of relative quietude. We see here 'collisional'

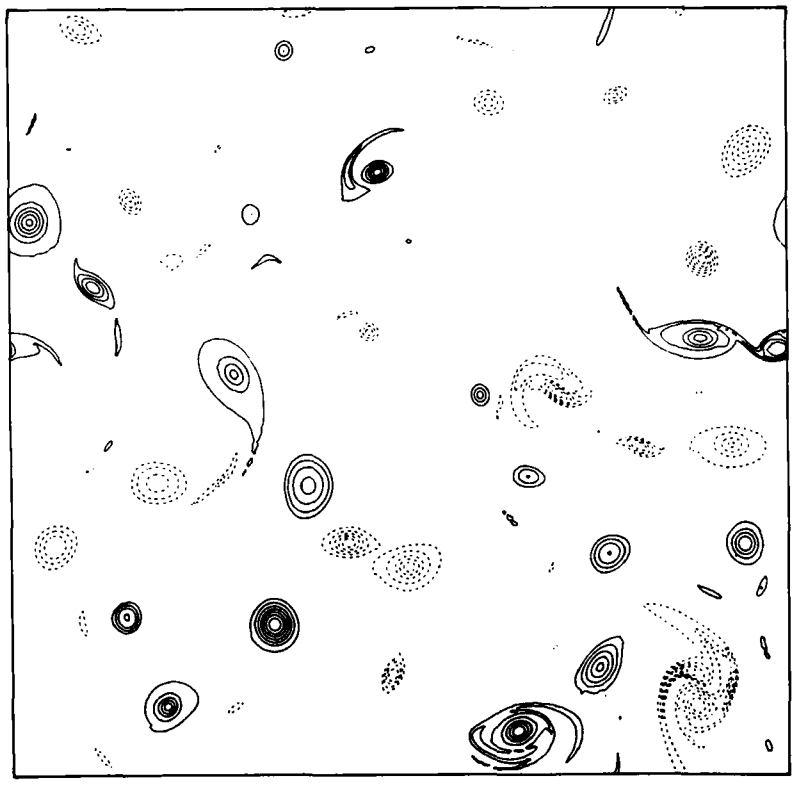

FIGURE 10. The vorticity field in physical space for case 3 at $t = 10$. After McWilliams (1984). Positive contours are solid, negative are dashed, and the contour interval is 5.

events in which like-signed vortex elements merge, extruding armlike structures, which wrap around. Mergers both generate larger vortices and dissipate enstrophy. Eventually the wraparounds heal (by dissipative axisymmetrization), leaving isolated circular vortex elements.

Concerning the large DNS–TFM discrepancy found here, three points may be made. First, it may be argued that the strong departure from Gaussianity may be associated with the use of a hyperviscosity (see e.g. (2)). Notice in this connection that the effect of the 'dissipation' operator (2) – acting alone – does not imply a monotonically decreasing kurtosis, as would be the case for Newtonian or Rayleigh dissipation. We have checked this point by rerunning both the DNS and TFM for case 3, but with a standard Newtonian viscosity. The results were virtually the same as with (2): the kurtosis of the DNS similarly increases, with the associated development of coherent structures; and the disagreement with the TFM is quite similar. We do not produce the graphical comparison here, for brevity.

Secondly, with regard to other theoretical approaches, it is of course possible that a more elaborate statistical closure – such as the Lagrangian-history closure (Kraichnan 1965) – will produce more satisfying results. However, other comparisons (Herring & Kraichnan 1979) of these methods in two dimensions indicated an indifferent improvement over the TFM – at least for short times. The velocity-based Lagrangian theory gave an energy and enstrophy transfer larger than the TFM, and hence we would expect its errors for the present study to be larger. The strain-based

Lagrangian-history theory did yield a smaller energy and enstrophy flux. This would suggest a modest improvement for the present study, but the agreement at smaller Reynolds number is not as satisfactory as for the TFM. In general, however, we would not expect a major change in the discrepancy between DNS and these other closure theories. Further, the agreement (case 1) and discrepancies (cases 2 and 3) are consistent with the geometry and physics of the flow: large TFM errors go with large K_ξ, and *vice versa*.

Thirdly, we have found that the TFM may be brought much closer into coincidence with the DNS by allowing the pressure-scrambling efficiency constant g^2 (here $= 0.60$) to increase as a function of Reynolds number. For example, we may take the excess of g^2 above its low-Re value (0.60) to be proportional to the excess of vorticity kurtosis above its Gaussian value of 3. This would – in part – simulate the fact that the coherent structures, which progressively dominate with increasing Re, arrest the transfer to large scales. We recall in this connection that the TFM's estimate for the duration of the strain process that accounts for the energy and enstrophy transfer is proportional to g^2: a small strain time is indicated by the fact that the regions of high strain occupy progressively smaller regions of space as Re increases. We mention this point here simply to reinforce the idea that the TFM disparity with respect to the DNS is consistent with the development of intermittent behaviour in the latter, and the inability of the former to represent strongly non-Gaussian behaviour adequately.

4. Prospects and concluding remarks

Our conclusions regarding the applicability of closures are somewhat narrowly focused in that we are unable to say quantitatively how much disruption of the tendency to form isolated vortices is needed to make the TFM accurate. If the validity of the closure is to be judged by the near-normality of the vorticity kurtosis, then it is of interest to observe that the presence of sufficient beta-effect or random topography suffices to limit it to near-Gaussian values (Holloway 1984; McWilliams 1984*a*, 1984*b*). This is true even in the absence of random forcing.

The comparisons of DNS with closures presented here may be of value in giving a quantitative characterization of the discrepancy between a non-Gaussian theory and numerical simulations which are, in varying degrees, non-Gaussian and hence intermittent. The latter attribute appears in the DNS in two (perhaps independent) guises: (1) the inertial-range intermittency (associated with the large-scale coherent structures) and (2) the dissipation-range intermittency, whose physics has been described by Kraichnan (1967) and in considerably more detail by Frisch & Morf (1981). The dissipation-range intermittency is most manifest here in case 1(*b*), although its numerical significance in reducing $E(k)$ below the TFM level is obscured by the arbitrary choice of g in the TFM. (The choice $g = 1$ would decrease the TFM spectrum in the dissipation range by about 20 %.)

One interesting aspect of the DNS is that, in all cases investigated here, the value of K_ψ remained nearly Gaussian. This suggests the possibility that closure could be useful in predicting large-scale phenomena such as eddy transport which depend sensitively only on the large scales where ψ-variance is centred. This may be so, but the flow at very large scales does depend on the smaller – isolated-vortex range – scales, particularly when the great majority of vorticity in the flow resides in the coherent vortices. Hence a closure calculation that ignored entirely the latter range would be wrong.

The DNS calculations reported here suggest a flow comprised at times large compared with the time of maximum-enstrophy dissipation of highly organized, isolated vortices, which cascade to dissipation only on the occasion of rare close encounters (which often lead to some degree of merger). The random elements are the vortex spacing and time of encounters. This differs markedly from the more familiar picture of chaotic, persistently dissipative turbulent flow.

The National Center for Atmospheric Research is sponsored by the National Science Foundation.

REFERENCES

BASEDEVANT, C., LEGRAS, B., SADOURNY, R. & BELAND, B. 1981 A study of barotropic model flows: intermittency, waves and predictability. *J. Atmos. Sci.* **38**, 2305.

BRACHET, M. E. & SULEM, P.-L. 1984 Direct numerical simulation of two-dimensional turbulence. In *Proc. 4th Beer Sheva Seminar on MHD flows and Turbulence.*

FORNBERG, B. 1977 A numerical study of 2-d turbulence. *J. Comp. Phys.* **25**, 1.

FRISCH, U. & MORF, R. 1981 Intermittency in nonlinear dynamics and singularities for complex times. *Phys. Rev.* **A 23**, 2673.

FRISCH, U. & SULEM, P.-L. 1984 Numerical simulation of the inverse cascade in two-dimensional turbulence. Preprint.

HAIDVOGEL, D. B. 1984 Particle dispersal and Lagrangian vorticity conservation in models of beta-plane turbulence. In preparation.

HERRING, J. R., ORSZAG, S. A., KRAICHNAN, R. H. & FOX, D. G. 1974 Decay of two-dimensional homogeneous turbulence. *J. Fluid Mech.* **66**, 417–466.

HERRING, J. R. & KRAICHNAN, R. H. 1979 A numerical comparison of velocity-based and strain-based Lagrangian-history turbulence approximations. *J. Fluid Mech.* **91**, 581–597.

HOLLOWAY, G. 1984 Contrary roles of planetary wave propagation in atmospheric predictability. In *Proc. La Jolla Inst. Workshop on Predictability of Fluid Flows* (ed. G. Holloway & B. West), pp. 593–600. New York: AIP.

KRAICHNAN, R. H. 1965 Lagrangian-history closure for turbulence. *Phys. Fluids* **8**, 575.

KRAICHNAN, R. H. 1967 Intermittency in the very small scales of turbulence. *Phys. Fluids* **10**, 2080–2082.

KRAICHNAN, R. H. 1971 An almost-Markovian Galilean-invariant turbulence model. *J. Fluid Mech.* **47**, 513–524.

KRAICHNAN, R. H. 1975 Statistical dynamics of two-dimensional flow. *J. Fluid Mech.* **67**, 155–175.

LILLY, D. K. 1969 Numerical simulation of two-dimensional turbulence. *Phys. Fluids Suppl. II* **12**, 240–249.

MCWILLIAMS, J. C. 1984*a* The emergence of isolated coherent vortices in turbulent flow. In *Proc. La Jolla Inst. Workshop on Predictability of Fluid Flows* (ed. G. Holloway & B. West), pp. 205–221. New York: AIP.

MCWILLIAMS, J. C. 1984*b* The emergence of isolated, coherent vortices in turbulent flow. *J. Fluid* solution in a β-plane channel. *J. Phys. Oceanogr.* **11**, 921–949.

ORSZAG, S. A. 1974 Statistical theory of turbulence. In *Proc. 1973 Les Houches Summer School* (ed. R. Balian & J.-L. Peaube), p. 237. Gordon & Breach.

SIGGIA, E. D. & AREF, H. 1981 Point vortex simulation of the inverse cascade in two-dimensional turbulence. *Phys. Fluids* **24**, 171–173.